

# PCCP

Accepted Manuscript



This is an *Accepted Manuscript*, which has been through the Royal Society of Chemistry peer review process and has been accepted for publication.

*Accepted Manuscripts* are published online shortly after acceptance, before technical editing, formatting and proof reading. Using this free service, authors can make their results available to the community, in citable form, before we publish the edited article. We will replace this *Accepted Manuscript* with the edited and formatted *Advance Article* as soon as it is available.

You can find more information about *Accepted Manuscripts* in the [Information for Authors](#).

Please note that technical editing may introduce minor changes to the text and/or graphics, which may alter content. The journal's standard [Terms & Conditions](#) and the [Ethical guidelines](#) still apply. In no event shall the Royal Society of Chemistry be held responsible for any errors or omissions in this *Accepted Manuscript* or any consequences arising from the use of any information it contains.



Journal Name

ARTICLE

## Photoacids as a new fluorescence tool for tracking structural transitions of proteins: Following the concentration-induced transition of bovine serum albumin

Received 00th January 20xx,  
Accepted 00th January 20xx

DOI: 10.1039/x0xx00000x

www.rsc.org/

Nadav Amdursky<sup>a</sup>

Spectroscopic-based techniques for assessing structural transitions of proteins follow either an intramolecular chromophore, as in absorption-based circular dichroism (CD) or fluorescence-based tryptophan emission, or an intermolecular chromophore such as fluorescent probes. Here a new fluorescent probe method to probe structural transition of proteins by photoacids is presented, which has a fundamentally different photo-physical origin to that of common fluorescent probes. Photoacids are molecules that release a proton upon photo-excitation. By following the steady-state and time-resolved emission of the protonated and de-protonated species of the photoacid we probe the environment of its binding site in bovine serum albumin (BSA) in a wide range of weight concentrations (0.001-8%). We found a unique concentration-induced structural transition of BSA at pH2 and at concentrations of >0.75%, which involves the exposure of its hydrophobic core to the solution. We confirm our results with the common tryptophan emission method, and show that the use of photoacids can result in a much more sensitive tool. We also show that common fluorescent probes and the CD methodologies have fundamental restrictions that limit their use in a concentration-dependent study. The use of photoacids is facile and requires only a fluorospectrometer (and preferably, but not mandatorily, a time-resolution emission system). The photoacid can be either non-covalently (as in this study) or covalently attach to the molecule, and can be readily employed to follow the local environment of numerous (bio-)systems.

### Introduction

How structural transitions of proteins change in various conditions is one of the fundamental questions in biochemistry. There are several spectroscopic methodologies that are commonly used to follow these transitions (folding/unfolding of proteins), which are based either on an intramolecular chromophore or an intermolecular one. The most frequently used methods that are based on an intramolecular chromophore are: 1) Circular dichroism (CD) that measures the difference in the absorption between right- and left-circularly polarized light of the carbonyl chromophore of the peptide bond, which is highly sensitive to the structure of the protein.<sup>1-3</sup> 2) Fourier transform Infrared spectroscopy (FTIR) that measures the IR absorption of vibrational modes in the molecule, in which for proteins it is mainly the vibration of the amide I bond (C=O stretching, 1600-1700 cm<sup>-1</sup>).<sup>4, 5</sup> The main limitation in FTIR measurements of proteins is the necessity of drying the protein or pelleting in potassium bromide, due to the strong IR excitation of water molecules.

This limitation can be overcome by using the less common Raman spectroscopy (mainly due to its cost and robustness) to determine the secondary structure of proteins.<sup>6, 7</sup> 3) The fluorescence of tryptophan (Trp), as the emission position of Trp is highly sensitive to the polarity of its environment, where the peak position can shift from 308 nm in a hydrophobic environment to 355 nm when it is exposed to water.<sup>8-10</sup> The use of Trp as an intramolecular probe relies on the protein having a Trp residue, and preferably only one, as multiple Trp residues can complicate the interpretation of the measurement. Other methodologies of intramolecular chromophores include the use of NMR,<sup>11</sup> small-angle X-ray scattering (SAXS)<sup>12</sup> and electron paramagnetic resonance spectroscopy,<sup>13</sup> though these techniques are not easy to interpret and/or not accessible to most researchers.

The spectroscopic methods that are based on an intermolecular probe (a probe that binds to the protein and is not the natural cofactor of it) can be divided to two main methods: 1) Förster (or fluorescence) resonance energy transfer (FRET), which describes a process where the light excitation of a donor chromophore induces the radiative fluorescence of an acceptor chromophore. The efficiency of FRET is proportional to  $r^{-6}$ , where  $r$  is the distance between the chromophores, thus minor changes in this distance dramatically affect the measured fluorescence FRET efficiency, hence its large sensitivity. FRET can be used to study interactions

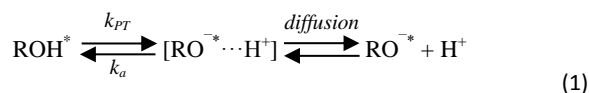
<sup>a</sup> Departments of Materials and Bioengineering, Imperial College London, London, SW7 2AZ, United Kingdom.

E-mail: n.amdursky@imperial.ac.uk

Electronic Supplementary Information (ESI) available: [Experimental, supplemental tables and Figures]. See DOI: 10.1039/x0xx00000x

between proteins<sup>14</sup> or between a protein and a nanoparticle,<sup>15</sup> and it can be also used to measure changes in protein structure.<sup>16-18</sup> In order to use FRET to follow structural changes of proteins one should incorporate both the donor and acceptor to the protein in specific locations (usually by site-specific mutagenesis). 2) Molecular probes that change their fluorescence intensity upon binding to proteins. This class of intermolecular probes include a wide variety of molecules, where the common ones are naphthalene sulfonate derivatives, thioflavins, Nile Red, rhodamines, squaraines and cyanines.<sup>19, 20</sup> Although there is large variability in intermolecular probes, the increase in the steady-state fluorescence and the radiative lifetime of all of the latter probes share similar photo-physical origin, where the increase in their fluorescence intensity is due to the inhibition of a non-radiative charge-transfer state from the electronically excited state to the ground state.

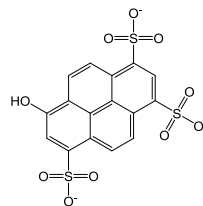
Here we present a new type of molecular probe to follow structural transitions of proteins by the use of photoacids. Similar to the use of the latter molecular probes for following structural changes of proteins, the use of photoacids also requires measuring the fluorescence of the molecule, but it has a completely different photo-physical origin. Photoacids are molecules that have different  $pK_a$  values between their electronically excited and ground states. For instance, for the photoacid that we use in this study, 8-hydroxy-1,3,6-pyrenetrisulfonate (HPTS, Scheme 1), the  $pK_a$  values are 7.4 and 1.3 for the ground and excited states, respectively. Accordingly, after the optical excitation of the molecule, its proton dissociates and the excited state can be described as:



where after the excitation the proton dissociates with a proton transfer rate constant of  $k_{PT}$ , to form an ion pair with the deprotonated acid. Following this stage, the proton can either undergo geminate recombination with the molecule to reform the  $\text{ROH}^*$  form with a geminate recombination rate of  $k_a$ , or diffuse away from the molecule, a process that is best described by the Debye–Smoluchowski equation.<sup>21</sup> Hence, if the photoacid is in water, the proton will diffuse rapidly to bulk water, and the  $\text{RO}^{\bullet-}$  form will be the predominate one. On the other hand, when the photoacid exists in a hydrophobic environment or next to an organic phase, the proton transfer rate will be slow with limited diffusion, thus the  $\text{ROH}^*$  form will tend to be the predominate one. Since the  $\text{ROH}^*$  and  $\text{RO}^{\bullet-}$  forms have different emission wavelengths (430 and 511, respectively) it is easy to distinguish between the two forms by steady-state fluorescence. Time-resolved fluorescence can also be used in conjunction with the steady-state results, for better analysis and understanding of the results. Recently it was shown that photoacids could be also used to probe the water accessibility of biological surfaces,<sup>22-24</sup> distinguishing between hydrophobic surfaces of amyloid fibrils and surfaces of polysaccharides that absorb water. In this study we show that HPTS can be used as a superior probe (in comparison to other

inter- and intra-molecular probes) for observing structural transition of proteins by following the structural transition of bovine serum albumin (BSA) at different pH values and as a function of concentration.

**Scheme 1.** Molecular structure of HPTS



## Experimental

**Sample preparation** – BSA (Sigma-Aldrich, ≥96%) was weighed and dissolved in either the acidic buffer (75mM NaCl, pH2, titrated with HCl) or the neutral buffer (2mM  $\text{Na}_2\text{HPO}_4$ , 75mM NaCl, pH7). Stock solutions of 10 and 40mM HPTS (Sigma-Aldrich, ≥97%), 10 and 70mM ANS (Sigma-Aldrich, ≥97%) and 10mM ThT (Sigma-Aldrich, 65-75%) were prepared in water (HPTS) or in DMSO (ANS and ThT). An aliquot from the stock solutions was placed in a 1mL BSA solution (or the reference sample of the buffer) for a final concentration of 20 or 170 $\mu\text{M}$  for HPTS, 30 or 300 $\mu\text{M}$  for ANS and 30 $\mu\text{M}$  for ThT. The BSA solutions with the molecular probe were placed at room temperature with mild shaking for 2h before measuring their fluorescence.

**Steady-state emission** – A Fluorolog system (Horiba) was used for the steady-state measurements. The samples were excited at 390, 380 and 435 nm for the excitation of HPTS, ANS and ThT, respectively. The entrance (excitation) and exit (emission) bandpass slits were 1 and 1nm, respectively for the 20 $\mu\text{M}$  HPTS, 30 $\mu\text{M}$  ANS and 30 $\mu\text{M}$  ThT samples and 1 and 0.5nm, respectively, for the 170 $\mu\text{M}$  HPTS and 300 $\mu\text{M}$  ANS samples. For Trp excitation, the BSA samples (without the molecular probe) were excited at 290 nm, and the entrance and exit bandpass slits were varied between 1-3nm for both sides to account for the different BSA concentrations.

**Time resolved emission** – A Deltaflex system (Horiba) was used to follow the time resolved emission spectrum of the samples containing HPTS. A 405 nm diode laser with a pulse duration of <100 ps was used as the excitation source. The emission was collected at two wavelengths: 440 and 530 nm, for the  $\text{ROH}^*$  and  $\text{RO}^{\bullet-}$  forms, respectively, where at least 20,000 counts were collected for the  $\text{ROH}^*$  form and 10,000 counts for the  $\text{RO}^{\bullet-}$  form in each measurement.

**Circular dichroism measurements** – A JASCO spectrometer was used to monitor the CD absorption signal of the BSA samples. Different cuvettes with pathlengths of 1, 0.01 and 0.01mm were used for the different BSA weight concentrations.

## Results and Discussion

### Steady-state emission of HPTS

We firstly measured the steady-state emission of HPTS in the presence of BSA in a wide range of weight concentration (from 0.001 to 8% w/v, which corresponds to 0.15  $\mu\text{M}$  and 1.2 mM or 0.1 and 80 mg/mL of BSA, respectively) at two pH values (pH7, Fig. 1, and pH2, Fig. 2) and with two HPTS concentrations of 20 and 170  $\mu\text{M}$ . The latter concentrations of HPTS correspond to BSA weight fractions of 0.13% and 1.1%, respectively. We show the steady-state emission as a normalized spectra, where the intensity of the  $\text{RO}^*$  peak was normalized to 1. Since HPTS is a photoacid, it has different steady-state emission at different pH values, where the lower the pH the higher the intensity of the  $\text{ROH}^*$  peak (Fig. 1 and 2, black curves). This is due to the large concentration of hydronium ions in lower pH values, which increases the probability for a geminate recombination process. Nevertheless, both in pH7 and pH2, the predominant population is that of the  $\text{RO}^*$  (only the ratio between  $\text{ROH}^*$  and  $\text{RO}^*$  changes). At pH7 (Fig. 1), the  $\text{ROH}^*$  peak intensity (at  $\sim 430$  nm) is similar to that of HPTS in buffer at low BSA concentration up to a certain concentration threshold (0.01% and 0.1% BSA for HPTS concentrations of 20, Fig. 1a, and 170  $\mu\text{M}$ , Fig. 1b, respectively and Fig. 3). From this concentration threshold, the effect of bound HPTS inside the BSA binding site can be clearly observed as a steady increase in the intensity of the  $\text{ROH}^*$  peak until all the HPTS molecules are bound to BSA (at  $\sim 0.5\%$  and  $2\%$  BSA for HPTS concentrations of 20 and 170  $\mu\text{M}$ , respectively). The un-normalized increase and decrease in the  $\text{ROH}^*$  and  $\text{RO}^*$  peaks, respectively, can be seen in Fig. S1, showing a clear isosbestic point at 468 nm. The increase in the normalized  $\text{ROH}^*$  peak is due to the binding of HPTS by BSA that limits the water accessibility of the HPTS molecule, reducing its excited state proton transfer (ESPT) rate which results in a more intense  $\text{ROH}^*$  peak. Increasing the BSA concentration above this point caused no significant change in the normalized intensity of the  $\text{ROH}^*$  peak. Though it is not known to which binding site of BSA HPTS can bind to, the hydrophobic pyrene core together with the negatively charged sulfonates make several hydrophobic and positively charged sites as possible binding sites for HPTS. Further crystal structure analysis is needed to resolve which binding site of BSA is the one for HPTS.

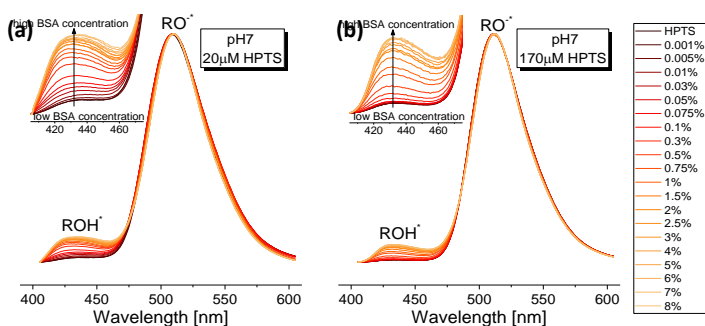


**Figure 1.** Normalized steady-state emission of (a) 20  $\mu\text{M}$  and (b) 170  $\mu\text{M}$  at pH7 in buffer and in different BSA weight concentration. The insets are a magnification of the  $\text{ROH}^*$  band. The y-axis is normalized intensity to the  $\text{RO}^*$  peak intensity.

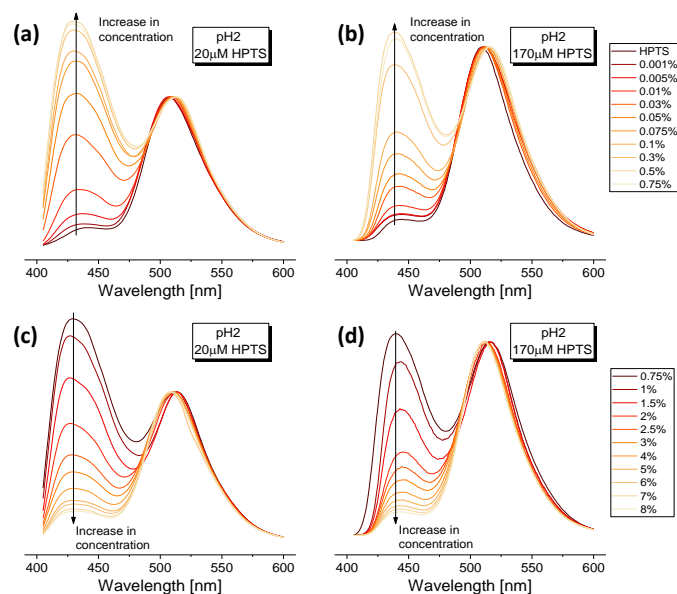


**Figure 2.** Normalized steady-state emission of (a and c) 20  $\mu\text{M}$  and (b and d) 170  $\mu\text{M}$  at pH2 in buffer and in different BSA weight concentration at the range of (a and b) 0.001-0.75% and (c and d) 0.75-8%. The y-axis is normalized intensity to the  $\text{RO}^*$  peak intensity.

As in the measurements in pH7, at pH2 the normalized  $\text{ROH}^*$  peak intensity is similar to the one of HPTS in the acidic buffer at low BSA concentration up to a concentration threshold, which is even lower than the one observed at pH7 (0.001% and 0.01% BSA for HPTS concentrations of 20, Fig. 2a, and 170  $\mu\text{M}$ , Fig. 2b, respectively). The un-normalized increase and decrease in the  $\text{ROH}^*$  and  $\text{RO}^*$  peaks, respectively, can be seen in Fig. S2. The increase in the intensity of the  $\text{ROH}^*$  peak of HPTS above certain BSA concentration indicates that similarly to the measurements at pH7, at pH2 HPTS can be also bound to BSA. Several studies showed the reversible structural transition of BSA (or the human form, HSA) at  $\sim \text{pH}2$ , which involves the loss of tertiary structure in what is known as the F $\rightarrow$ E transition of the protein.<sup>25-28</sup> Hence our finding indicates that even when the BSA protein has been considered as losing its tertiary structure, it has 'active' binding sites that can bind small molecules. However, unlike the measurements at pH7 (Fig. 1), the increase in the intensity of the  $\text{ROH}^*$  peak at pH2 does not saturate at a certain BSA concentration, but starts to decrease after a second concentration threshold ( $\sim 0.75\%$ ), both for the low (Fig. 2c) and high (Fig. 2d) HPTS concentrations (The un-normalized spectra can be seen in Fig. S2). Following this second concentration threshold, the  $\text{ROH}^*$  peak intensity decreases with intensity up to the point where at the highest measured BSA concentration of 8%, its intensity almost resembles that of HPTS (without protein) in the same buffer. As will be discussed below, the normalized intensity of the  $\text{ROH}^*$  peak is an indicator for the environment of HPTS. Thus, the decrease in the  $\text{ROH}^*$  peak intensity after a certain BSA concentration and only at pH2 points out that BSA undergoes a second structural transition which is a concentration induced one. Unlike the first structural transition at pH2 (the F $\rightarrow$ E transition) that does not affect the

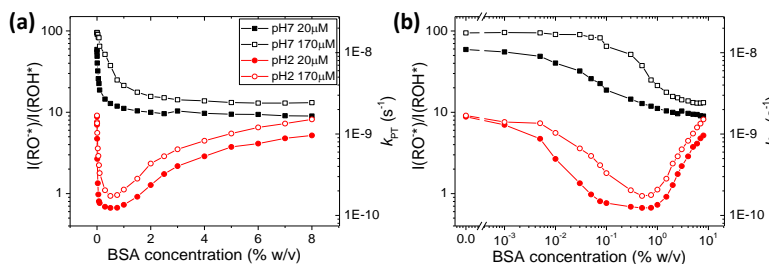


**Figure 3.** The change in the  $I_{RO^-}^F/I_{ROH}^F$  ratio (left y-axis) and in the corresponding  $k_{PT}$  values (right y-axis) of HPTS at pH7 (solid and empty black squares for the concentrations of 20 and 170  $\mu\text{M}$ , respectively) and pH2 (solid and empty red circles for the concentrations of 20 and 170  $\mu\text{M}$ , respectively) as a function of BSA concentration on (a) a semi-logarithmic scale and (b) log-log scale. Panel (b) does not show the point of only HPTS solution (0% BSA), as the x-axis is a logarithmic one.

binding of HPTS to BSA, the second transition causes a significant change in the binding site configuration, which either release the bound HPTS to solution, or completely expose the site to solution.

The change in the ratio between the  $ROH^*$  and  $RO^-*$  peaks is a result of a different proton transfer rate constant ( $k_{PT}$ , Eq. 1) of HPTS, as it is known that the ESPT of HPTS is slower when the proton acceptor is an organic phase (such as the BSA protein) and not water.<sup>23, 24, 29</sup> An approximation for  $k_{PT}$ , while excluding back-reactions (geminate recombination), can be approximated by using the following simple relation:

$$k_{PT} \approx \frac{I_{RO^-}^F}{I_{ROH}^F} \cdot \tau_{RO^-}^{-1} \quad (2)$$

where  $I_{RO^-}^F$  and  $I_{ROH}^F$  are the fluorescent intensity of the  $RO^-*$  and  $ROH^*$  peaks and  $\tau_{RO^-}^{-1}$  is the inverse of the  $RO^-*$  radiative decay, which is  $\sim 5.4$  ns. Figure 3 shows the ratio of  $I_{RO^-}^F/I_{ROH}^F$  and the approximated proton transfer rate of HPTS in water and in the presence of the different BSA concentrations at the two pH values and with the two HPTS concentrations (Table S1 displays all the values for  $k_{PT}$ ). As can be seen in Figure 3 and Table S1, at pH7 the  $k_{PT}$  values and the  $I_{RO^-}^F/I_{ROH}^F$  ratio decrease as function of BSA concentration until they reach a value  $\sim 7.4$  times lower than that of HPTS in the same buffer and concentration. At pH2, the  $k_{PT}$  values and the  $I_{RO^-}^F/I_{ROH}^F$  ratio are an order of magnitude lower than at pH7, as expected from the higher concentration of hydronium ions in the solution. Similar to the results at pH7, at pH2 the  $k_{PT}$  values and the ratio decrease as a function of BSA concentration but only to a concentration of 0.75% (w/v), at which point the values are  $\sim 10$ -13 times lower than that of HPTS in the same acidic buffer. As discussed above, the steady-state results indicate that above 0.75% the protein undergoes a concentration-induced structural transition which expose the binding site to the solution, and subsequently induces an increase in the  $k_{PT}$  values and the  $I_{RO^-}^F/I_{ROH}^F$  ratio up to their approximate original value at the lowest measured BSA concentration. The exposure of the BSA binding site at low pH

values and at high BSA concentrations is supported by the BSA fibril formation mechanism suggested by Mukhopadhyay and coworkers.<sup>30, 31</sup> In their model they propose that at low pH values the native state of BSA transform into a 'molten-globule-like expanded state', which can then be transformed into 'molten oligomers' at high BSA concentrations, and upon heating the oligomers can aggregate into the fibril structure. Our conclusion is also supported by the results of Barbosa et al.,<sup>32</sup> who studied conformational changes of BSA by SAXS. As part of their study they measured the SAXS signal of BSA at the weight concentrations of 1, 2.5 and 5% and at different pH values. They found that while at pH7 BSA does not go any structural transition as function of concentration, at pH2 the protein undergoes a conformational change from the unfolded structure at 1% concentration to a more globular conformation at higher weight concentrations, a conformation that cannot be considered as a refolding of the protein. Their conclusion is in perfect agreement with the present results.

#### Time-resolved emission of HPTS

In order to complement the steady-state measurements, we also performed time-resolved measurements of HPTS fluorescence (at 170  $\mu\text{M}$ ) in the presence of the different BSA concentrations and at different pH values. Since the  $ROH^*$  and  $RO^-*$  forms of HPTS emit at different wavelengths it allows to follow the decay of the two forms separately. In general, the decay of  $ROH^*$  (Fig. 4a-b) in water consists of a fast decay in the first nanoseconds that is a result of the fast ESPT process of HPTS ( $k_{PT}$  in Eq. (1)), followed by a long-lived tail that is the results of the geminate recombination process of HPTS ( $k_a$  in Eq. (1)).<sup>21, 29</sup> At pH7 (black curves in Fig. 4a-b), the fast initial decay, which is the result of the efficient ESPT of HPTS in

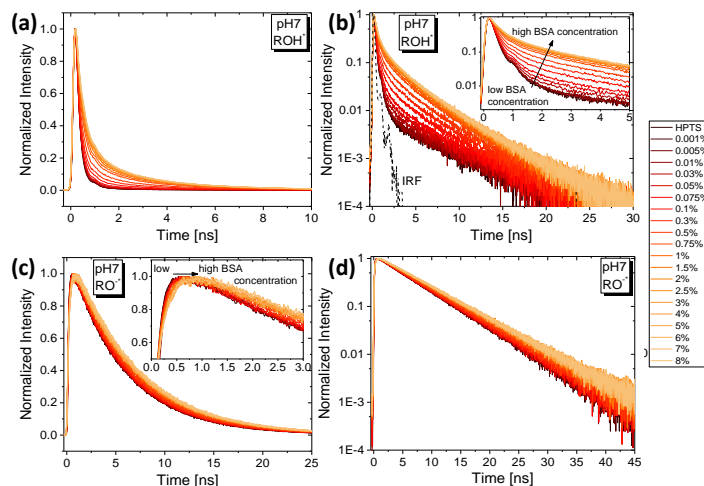


**Figure 4.** Time-resolved emission of HPTS at pH7 at the emission wavelengths of  $ROH^*$  (a and b, displayed on a linear and semi-log scales, respectively) and  $RO^-*$  (c and d, displayed on a linear and semi-log scales, respectively) in different BSA concentrations. The insets of panels (b) and (c) are a magnification of the first nanoseconds. The dashed line in panel (b) is the instrumental response function (IRF) of the light source.

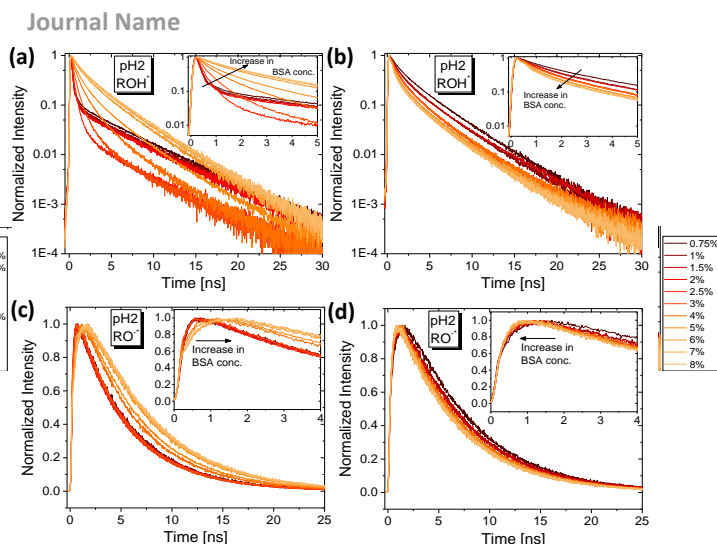


**Figure 5.** Time-resolved emission of HPTS at pH2 at the emission wavelengths of ROH\* (a and b, on a semi-log scale, the linear scale is in Fig. S1) and RO-\* (c and d, on a linear scale, the semi-log scale is in Fig. S2) in BSA fractions of  $\leq 0.75\%$  (a and c) and  $\geq 0.75\%$  (b and d). The insets are a magnification of the first nanoseconds.

water, consists of more than 99% of the signal. As the BSA concentration of the solution was increased we can clearly see an increase in the lifetime of the first initial decay, indicating on a slower proton transfer rate. This is consistent with our estimated  $k_{PT}$  values that were calculated from the steady-state measurements (Table S1). The ROH\* decay shape of HPTS in the presence of BSA is also very different than the one of HPTS in water as it is non-exponential, in comparison to the double-exponent decay of ROH\* in water. This non-exponentiality indicates that not only the ESPT efficiency is different, but also the geminate recombination rate of the protons inside the binding site of BSA and the diffusion of the protons from the binding site is different (see further discussion in References<sup>33,34</sup>). This fundamental change of the time-resolved spectra at low BSA weight fractions also indicates on the strong binding of HPTS to BSA.

An additional validation for the slower ESPT of HPTS inside BSA can be observed by following the RO-\* decay (Fig. 4c-d). Unlike the fast decay of the ROH\* form, the RO-\* has a long rise-time, followed by a long-lived exponential radiative decay of the RO-\* form. The rise-time is roughly proportional (but not always) to:  $\propto 1 - \exp(-k_{PT}t)$ . As can be seen in the inset of Fig. 4c, the rise-time is slightly increased as function of the BSA concentration, which further support the slower ESPT of HPTS inside BSA.

Figures 5 and S3 shows the ROH\* decay at pH2 (on a semi-logarithmic and linear scales, respectively). The ROH\* decay of HPTS at pH2 (black curve in Fig. 5) also consists of a fast decay as at pH7, but it consists of less than 90% of the signal (in comparison to 99% in pH7). This is due to the better geminate recombination rate at pH2, which can be observed as a high-intensity long-lived decay after  $\sim 1-1.5$  ns. Similar to the measurements at pH7, at pH2 the lifetime of the fast decay increases as function of BSA concentration, but as discussed above, only up to a BSA concentration of 0.75% (Fig. 5a and

Fig. S3a). Above the latter concentration, the lifetime of the fast decay decreases as a function of the BSA concentration (Fig. 5b and Fig. S3b). Interestingly, as soon as the lifetime of the fast decay increases (at BSA concentrations of  $>0.01\%$ ), the shape of the curve becomes non-exponential, and does not exhibit the pronounced double-exponential decay of HPTS in this acidic buffer. This finding points out that even at pH2, where BSA is known to be partially unfolded due to the F $\rightarrow$ E transition, the binding site of HPTS inside BSA ‘shields’ the HPTS molecule from the acidic buffer of the protein. As discussed above, the steady-state emission results could not distinguish between the release of the HPTS after the second structural transition ( $>0.75\%$  BSA) and a change in the binding site environment of HPTS in BSA. The time resolved emission measurements (Fig. 5b) clearly show that after the concentration-induced structural transition, HPTS is still bound to BSA since the shape of the decay remains non-exponential.

Similar to the measurements at pH7, the changes in the ESPT can also be observed by following the RO-\* decay (Fig. 5c-d and Fig. S4 on a linear and semi-logarithmic scales, respectively). At low BSA concentrations ( $<0.75\%$ ), the rise-time of the RO-\* signal (Fig. 5c and Fig. S4a) increases as function of BSA concentration, with a larger amplitude than observed at pH7 (Fig. 4c-d). Following the concentration-induced structural transition, this rise-time starts to decrease as a function of BSA concentration (Fig. 5d and S4b), indicating an increase in the proton transfer rate constant.

#### Steady-state emission of Trp

In the previous sections we discussed the unique concentration-induced structural transition of BSA at pH2 for weight fractions  $>0.75\%$ . This structural transition involves the exposure of the BSA binding site to the solution. In this work we would like to present HPTS as a novel method to follow structural transitions of proteins, thus in this section we wish to verify the concentration-induced structural transition of BSA at pH2 by the commonly used method of Trp emission (BSA has two Trp residues at positions 134 and 213). The fluorescence peak position of Trp is sensitive to the polarity of its environment, in which a hydrophobic environment results in a blue shift of the peak position, and vice versa, water exposed environments result in a red shift of the signal. The fluorescence intensity of the Trp residue is also sensitive to the environment of the amino acid, where exposure of the residue to water results in quenching of the fluorescence. However using the Trp fluorescence intensity as a marker for the environment of the residue in a concentration-dependence study with a very wide range of concentrations as in our study requires changing the entrance and exit slits of the fluorospectrometer. As such, the approach can be very misleading and is not recommended.

At pH7 (Fig. 6a), the Trp emission peak position does not exhibit a significant change as function of BSA concentration, where the peak position is located at  $343 \pm 2$  nm (Fig. 7). Nonetheless, there is a small blue shift of the Trp peak position at pH7 and at high BSA concentration ( $>1.5\%$ ), which suggest a

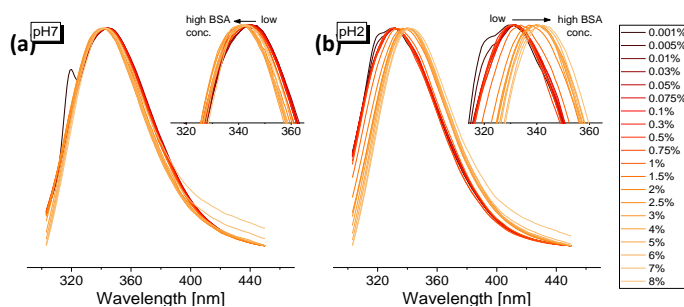


**Figure 6.** Normalized steady-state Trp emission of BSA at different weight fractions at (a) pH7 and (b) pH2. The insets show a magnification of the peak. The peak/shoulder at around 320 nm that present in the low BSA concentrations is associated to the Raman scattering of water.

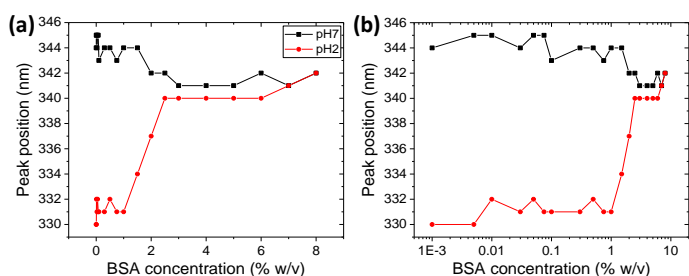


**Figure 7.** The change in the Trp peak position of BSA at pH7 (black curve) and pH2 (red curve) as function of BSA concentration on (a) a linear scale and (b) a semi-logarithmic scale.

slightly more hydrophobic environment of the Trp at these concentrations. The high BSA concentrations that were investigated in this study affect the viscosity of the solution, which can induce the observed small change in the Trp peak position, as observed for BSA and HSA solutions containing different anionic surfactants, where an increase in the solution viscosity induced a blue shift in the Trp emission.<sup>35</sup>

The F $\rightarrow$ E transition of BSA at pH2 involves a significant change in the protein secondary structure.<sup>25-28</sup> By following the Trp emission in this pH (Fig. 6b) we found that there is a significant blue shift in the emission peak of 13 $\pm$ 1nm in comparison to the peak position at pH7 at low BSA fractions of <1% (Fig. 7). This large blue shift of the peak position suggests that upon the F $\rightarrow$ E structural transition, the environment of the Trp becomes more hydrophobic (less water accessible). This is supported by the results of HPTS, where the differences in the  $k_{PT}$  values and the  $I_{RO}^E/I_{ROH}^E$  ratio between the bound HPTS (at 0.75% BSA) to free HPTS in the solution are larger at pH2 in comparison to pH7. This suggests that the HPTS binding site in BSA is less water accessible at pH2 in comparison to the binding site at pH7. The concentration-induced structural transition of BSA at pH2 was also observed by a significant change in the position of the Trp emission (Fig. 6b and Fig. 7), where a sharp red shift of the peak position was observed above 1% BSA. This red shift indicates that the Trp is more water accessible after the concentration-induced structural

transition. This result is in line with the results obtained with the use of the HPTS photoacid.

### Steady-state emission of common molecular probes

BSA is one of the most common proteins used to study the interaction between molecular probes and proteins, where the emission of numerous molecular probes has been shown to increase after binding to BSA (or HSA).<sup>19</sup> The most common molecular probe that was used for following structural transitions in BSA is 1-anilino-8-naphthalene sulfonate (ANS).<sup>36-39</sup> The increase in ANS steady-state fluorescence and lifetime is due to the binding of the dye to hydrophobic patches in BSA, although it might have some recently discovered limitations.<sup>40, 41</sup> An additional common probe that is used for following the aggregation of BSA is thioflavin-T (ThT).<sup>30, 42-44</sup> The increase in the probe fluorescence is due to the inhibition of the non-radiative charge transfer crossing between the excited and ground states of the molecule. This inhibition is due to the restriction of the free rotation usually around a single bond of the molecule after binding to the protein, either to the hydrophobic part of the protein as for ANS, or for the aggregated form of the protein as for ThT.<sup>45, 46</sup> In addition to the increase in the intensity, ANS also undergoes a steady-state solvatochromism, where the change in the dipole of the surrounded solvent (following the binding to the hydrophobic patch of the protein) induces a change in the steady-state emission peak position (blue-shift for ANS).

Herein we follow the change in the steady-state emission of both ANS and ThT. In line with previous studies,<sup>36-39</sup> we also find an increase in ANS fluorescence intensity upon binding to BSA (Fig. 8), accompanied by a blue shift of the signal (inset). At pH7 and at the ANS concentration of 30 $\mu$ M (Fig. 8a), which

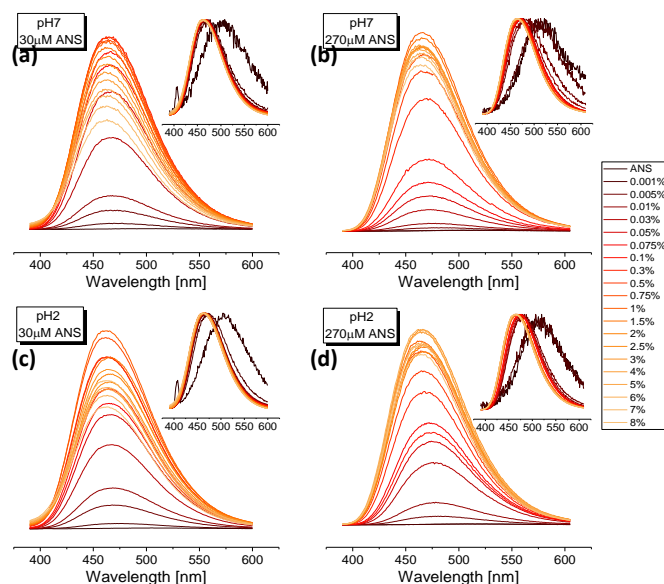


**Figure 8.** Steady-state emission of ANS in different BSA weight concentrations at (a and b) pH7 at ANS concentrations of (a) 30 $\mu$ M and (b) 270 $\mu$ M, and at (c and d) pH2 at ANS concentrations of (c) 30 $\mu$ M and (d) 270 $\mu$ M. The y-axis is the non-normalized intensity (counts) of fluorescence. The insets show the normalized emission.

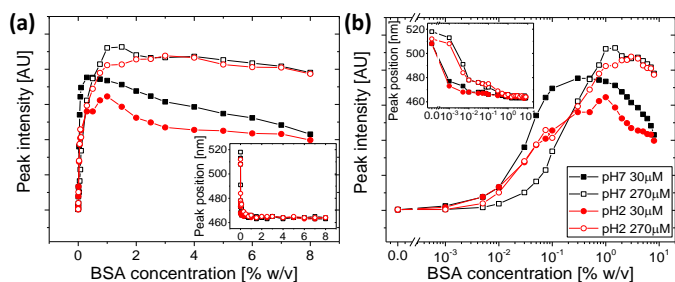


**Figure 9.** The change in ANS steady-state emission as function of BSA concentration at pH7 (black curve) and pH2 (red curve) for ANS concentrations of 30 and 270  $\mu\text{M}$  (solid and empty symbols, respectively) on (a) a linear scale and (b) a semi-logarithmic scale. The insets show the corresponding change in peak position.

corresponds to a BSA weight concentration of  $\sim 0.2\%$ , the increase in ANS fluorescence and shift in peak position (Fig. 9, solid black squares) was observed even at the lowest measured BSA weight concentration of 0.001%. As seen in the figure, the ANS fluorescence intensity increased as a function of the BSA concentration, but only up to BSA weight concentration of 0.3%, whereupon a drop in ANS fluorescence was observed. This drop in fluorescence is not due to any structural change of BSA in pH7, but it is simply quenching of the ANS fluorescence by BSA when the BSA concentration was larger than that of ANS. In order to validate our assumption we also used a much higher ANS concentration of 270  $\mu\text{M}$  (Fig. 8b), which corresponds to a BSA weight concentration of 2%. The high ANS concentration resulted in a slower increase in the dye fluorescence due to the large amount of unbound ANS molecules for the low BSA concentrations. The increase of ANS fluorescence (Fig. 9, empty black squares) at the high concentration of 270  $\mu\text{M}$  was only up to BSA weight concentration of 2%, in which a drop in the intensity was observed above this concentration, thus validating our assumption. At pH2 we observed a similar increase in ANS fluorescence as a function of BSA concentration accompanied by a decrease in the fluorescence at higher BSA concentration, both for the lower ANS concentration of 30  $\mu\text{M}$  (Fig. 8c), and for the higher concentration of 270  $\mu\text{M}$  (Fig. 8d). Since the ANS probe is known to prefer hydrophobic patches in proteins, we have expected that it will be suitable to follow the concentration-induced structural transition of BSA at pH2, which leads to an exposure of hydrophobic parts of the protein to the solution. However, since the ANS assay relies on monitoring the absolute emission of it (and not the ratio between the peaks as in photoacids), its quenching by the BSA molecules makes this assay unsuitable for concentration dependent studies. Nevertheless, as seen in Fig. 9 the quenching of ANS fluorescence at pH2 (red squares) starts at higher BSA concentrations than in pH7 (black squares), thus imply that indeed BSA at pH2 and at high BSA concentration expose its hydrophobic core to the solution, which subsequently increases the binding of ANS to the protein. In addition, we also followed the fluorescence of ThT (Fig. 10). Unlike ANS, which is known to bind to hydrophobic patches in

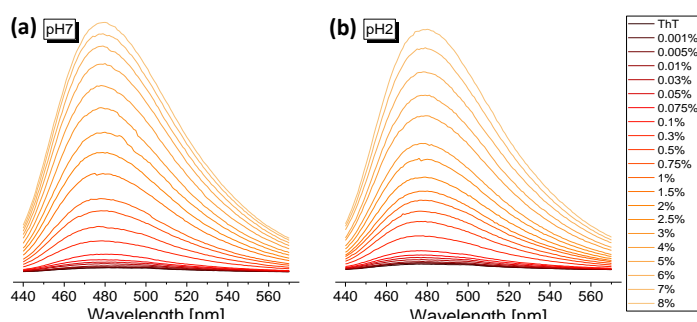


**Figure 10.** Steady-state emission of ThT (30  $\mu\text{M}$ ) in different BSA weight concentrations at (a) pH7 and at (b) pH2. The y-axis is the non-normalized intensity (counts) of fluorescence.

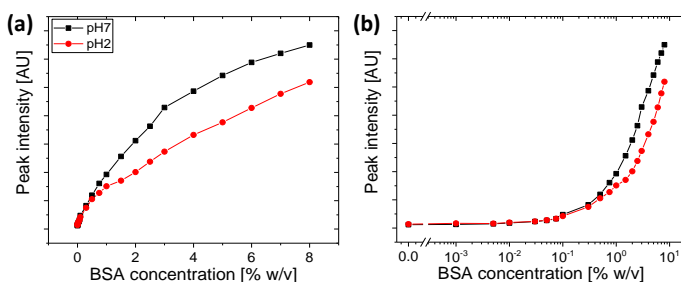


**Figure 11.** The change in ThT steady-state emission as a function of BSA concentration at pH7 (black curve) and pH2 (red curve) on (a) a linear scale and (b) a semi-logarithmic scale.

the protein, ThT is known to bind to aggregated form of proteins, mainly amyloid fibrils, and as such, it is mainly used to follow the aggregation of BSA and HSA.<sup>30, 42-44</sup> Nevertheless, we observed an increase in ThT fluorescence as function of BSA concentration both in pH7 (Fig. 10a) and in pH2 (Fig. 10b), which implies that ThT can bind also to the native form of the protein. However, unlike the change in ANS fluorescence, the increase in ThT fluorescence as a function of BSA concentration (Fig. 11) is not as sharp as in ANS, which implies that the binding of ThT to BSA is much weaker than the binding of ANS. Due to this weak binding between ThT and BSA, the fluorescence of ThT (Fig. 11) does not saturate and start to be quenched like that of ANS (Fig. 9), but rather continuously increases as a function of BSA concentration. The lack of substantial differences in the fluorescence of ThT as a function of BSA concentration between pH7 and pH2 implies that this probe is not suitable for the detection of the concentration-induced structural transition in BSA at pH2.

Even though there are many molecular probes for following structural transitions in proteins,<sup>19, 20</sup> they have similar photo-physical origin for their change in fluorescence, where the binding to the protein inhibits the nonradiative decay from the excited state to the ground state. This can be imagined as an on/off switch, where the binding of the dye to the protein light it up. However, as we show here for ANS, in a concentration-dependent study of the protein, the use of the absolute fluorescence of the probe, rather than the normalized one, might result in a misleading result which is due to quenching of the fluorescence, and not as a result of a change in the on/off states of the dye. Moreover, the on/off

fluorescence switch of the dye might obscure structural changes in the protein, for example, due to the weak binding of ThT to BSA, it lights up as a function of BSA concentration, regardless to the conformation of the BSA.

#### Circular dichroism measurements and artefacts of absorption-based techniques of protein intramolecular chromophores

In the last section we would like to emphasize the advantages of using a fluorescence intermolecular probe in comparison to following the absorption of an intramolecular chromophore for concentration-dependent type of measurements. As mentioned in the introduction, CD is one of the most used techniques to follow structural transitions of proteins. In general, for estimating the protein secondary structure motifs, the CD methodology measures the difference in the absorption between left- and right-handed circularly polarized light of the peptide bond carbonyl chromophore. The F→E transition of BSA and HSA was followed by CD,<sup>25, 26</sup> where it was found that the  $\alpha$ -helical structure of the protein is partially unfolded, accompanied by a decrease in the CD signal at the 220-222 nm region. In line with the latter studies, we also find similar differences between the CD signal of BSA at pH7 and pH2, at the low concentration region, comparable to the one that was used in the latter studies (Fig. 12).

We further followed the change in the CD spectrum at both pH7 (Fig. 13a-b) and pH2 (Fig. 13c-d). The CD signal is very sensitive to the absorption of the sample, hence it is important to choose an appropriate pathlength for the measurement. Since we conducted a concentration-dependent study, we had to use different pathlengths, spanning two orders of magnitude range from 1 to 0.01mm (the smallest commercially available quartz cuvette). At pH7 BSA is not undergoing a concentration-induced structural transition, and indeed we found that up to the weight concentration of 1% there is no change in the molar CD of the protein (Fig. 13a). However, above 1% the CD signal of the solution has significantly changed (Fig. 13b), even though a structural transition was not expected. This significant change in the CD signal is an example of the artefacts that can arise in absorption-based type of measurements, where the molar CD signal of a sample is significantly dropped at high absorbing samples, as the high concentrated samples in our study. Indeed, as can be seen in Fig. S5, the corresponded absorption of the solution >1% fractions crosses the absorption limit for a reliable CD measurement ( $\sim 1$  OD). The secondary structure of

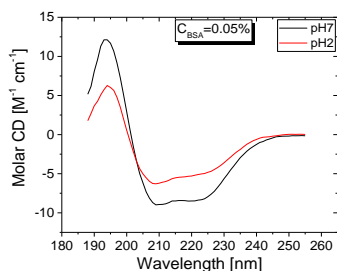


**Figure 12.** CD spectrum of BSA at weight fraction of 0.05% ( $\sim 7.5 \mu\text{M}$ ) at pH7 and pH2.

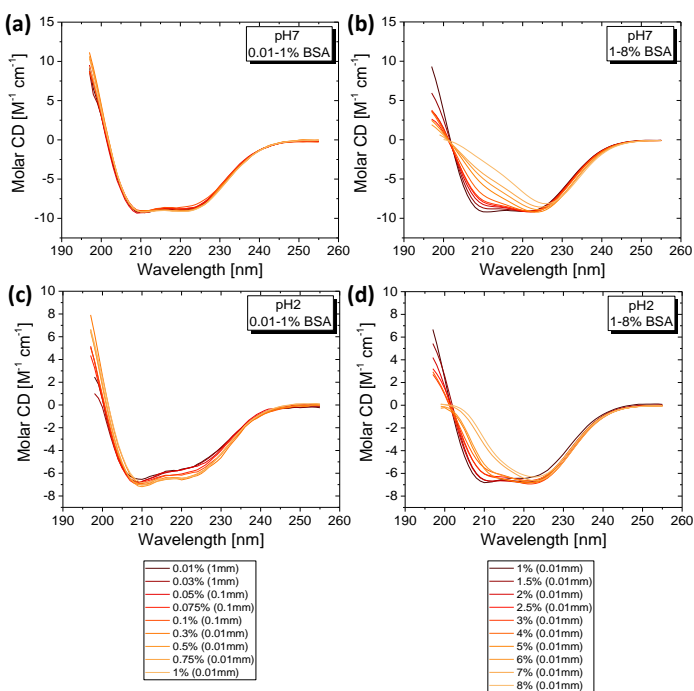


**Figure 13.** CD spectra of BSA at (a and b) pH7 and (c and d) pH2 at weight fractions  $\leq 1\%$  (a and c) and  $\geq 1\%$  (b and d). The brackets in the figure legends indicate the pathlength that was used for the measured concentration.

the protein can be estimated by bioinformatical tools.<sup>2</sup> We have used the K2D3 package<sup>47</sup> to estimate the secondary structure of BSA at pH7 at weight concentrations lower than 1% (Table S2). In line with previous studies<sup>48-50</sup> we have found that the  $\alpha$ -helical content of BSA at pH7 is  $68.0 \pm 0.2\%$ . The F→E transition of BSA is accompanied by a decrease in the  $\alpha$ -helical content of the protein.<sup>25, 26</sup> By using the same K2D3 package we also found a decrease of the  $\alpha$ -helical content of BSA at pH2 at low weight concentration (Table S2), though in lower magnitude to what was reported previously<sup>26</sup> (which might well be due to the use of a different bioinformatical package to calculate the secondary structure content from the CD spectrum). As displayed in Table S2, we do observe an additional significant decrease in the  $\alpha$ -helical content of the protein at the concentration of 1% at pH2, which might be related to the discussed concentration-induced structural transition at pH2 and at weight fractions  $>0.75-1\%$ . But, unfortunately, due to the discussed artefacts of the CD spectra (Figs. 13b and 13d), which is due to the high absorbance of the samples (Fig. S5), the spectra  $>1\%$  fractions should not be qualitatively interpreted.

It is important to note that, as similar to CD, the use of the Trp fluorescence to follow structural transitions in proteins also relies on an intramolecular chromophore. But unlike absorption-based measurements that depend on the pathlength of the solution, the emission of fluorescence-based techniques can be easily modified by changing the entrance and exit slits of a fluorospectrometer. Nevertheless, at high sample concentration the emission intensity of the solution is significantly affected by inner filter effect (these can be also

referred to as self-absorbance, and should not be confused with fluorescence quenching),<sup>51</sup> where the chromophores re-absorb the excitation light as well as the fluorescence, which subsequently causes a decrease in the emission. Due to this effect we recommend extreme caution in the use of the fluorescence intensity as the measurable parameter in a concentration dependent study. Unlike the intensity of emission which is significantly affected, the peak location or the ratio between peaks is not affected, and can be used as an index in a concentration dependent studies (as performed in this study).

## Conclusions

In summary, we have shown here the novel use of a photoacid (HPTS) in order to follow structural transitions in BSA. Upon light excitation the protonated photoacid ( $\text{ROH}^*$ ) releases a proton, which can either diffuse into water, be transferred to a nearby amino acid or geminate recombine with the deprotonated photoacid molecule ( $\text{RO}^-$ ). Since the  $\text{RO}^-$  and  $\text{ROH}^*$  forms have different emission bands, one can follow the excited state photocycle of the photoacid, which is very sensitive to the environment of the photoacid. We used the natural ability of BSA to bind small molecules in order to bind the HPTS molecule to the protein, but HPTS can be also covalently attached to surfaces.<sup>52</sup> By following the steady-state and time-resolved emission of the bound HPTS we could find a unique concentration-induced structural transition of BSA at the low pH value of 2 and at high BSA weight concentrations of >0.75% (w/v). Concentration-induced structural transition of proteins is commonly associated to the amyloidogenesis process of amyloid proteins.<sup>53-55</sup> We show that the structural transition of BSA at pH2 involves the exposure of the hydrophobic core to the solution. We further confirmed our findings with the more traditional method of monitoring the change in the emission peak position of Trp. However, while the changes in the Trp peak position are in the order of only few nanometres (either red- or blue-shift) between the 0.75% concentration to the highest measured concentration of 8%, the sensitivity of the photoacid is much larger, where the difference in the calculated proton transfer rate was almost an order of magnitude between these latter BSA concentrations. The use of a photoacid as a molecular probe for following structural transitions in proteins (or any other biomolecule), and especially for concentration-induced ones, is highly attractive since, unlike the concentration of the protein, the concentration of the photoacid is not changed. Hence fluorescence inner-filter effects can be avoided. Moreover, the results of the photoacid molecular probe were a significant improvement over the use of conventional fluorescence molecular probes, such as ANS and ThT, as the latter probes follow the fluorescence intensity of the probe and not the ratio between separate peaks in the steady-state spectrum. We also discuss how the use of photoacids in a concentration-dependent study is much more reliable in comparison to the absorption-based CD methodology, which was not applicable

when extending investigations into the high weight concentration regime.

## Acknowledgements

We thank M. M. Stevens for the use of her research lab and M. R. Thomas for critical reading. The research was supported by Marie Curie actions FP7 through the Intra-European Marie Curie Fellowship ConPilus under grant agreement no. 623123.

## Notes and references

- 1 S. M. Kelly, T. J. Jess and N. C. Price, *Biochim. Biophys. Acta, Proteins Proteomics*, 2005, **1751**, 119-139.
- 2 L. Whitmore and B. A. Wallace, *Biopolymers*, 2008, **89**, 392-400.
- 3 W. C. Johnson, *Proteins Struct. Funct. Genet.*, 1990, **7**, 205-214.
- 4 M. Jackson and H. H. Mantsch, *Crit. Rev. Biochem. Mol. Biol.*, 1995, **30**, 95-120.
- 5 D. M. Byler and H. Susi, *Biopolymers*, 1986, **25**, 469-487.
- 6 Z. H. Chi, X. G. Chen, J. S. W. Holtz and S. A. Asher, *Biochemistry*, 1998, **37**, 2854-2864.
- 7 J. L. Lippert, D. Tymiński and P. J. Desmeules, *J. Am. Chem. Soc.*, 1976, **98**, 7075-7080.
- 8 M. R. Eftink, *Biophys. J.*, 1994, **66**, 482-501.
- 9 J. M. Beechem and L. Brand, *Annu. Rev. Biochem.*, 1985, **54**, 43-71.
- 10 J. T. Vivian and P. R. Callis, *Biophys. J.*, 2001, **80**, 2093-2109.
- 11 M. Sattler, J. Schleucher and C. Griesinger, *Prog. Nucl. Magn. Reson. Spectrosc.*, 1999, **34**, 93-158.
- 12 H. D. T. Mertens and D. I. Svergun, *J. Struct. Biol.*, 2010, **172**, 128-141.
- 13 N. Alexander, A. Al-Mestarihi, M. Bortolus, H. McHaourab and J. Meiler, *Structure*, 2008, **16**, 181-195.
- 14 A. K. Kenworthy, *Methods*, 2001, **24**, 289-296.
- 15 A. R. Clapp, I. L. Medintz, J. M. Mauro, B. R. Fisher, M. G. Bawendi and H. Mattoussi, *J. Am. Chem. Soc.*, 2004, **126**, 301-310.
- 16 A. A. Deniz, T. A. Laurence, G. S. Belligere, M. Dahan, A. B. Martin, D. S. Chemla, P. E. Dawson, P. G. Schultz and S. Weiss, *Proc. Natl. Acad. Sci.*, 2000, **97**, 5179-5184.
- 17 J. W. Taraska, M. C. Puljung, N. B. Olivier, G. E. Flynn and W. N. Zagotta, *Nat. Meth.*, 2009, **6**, 532-537.
- 18 C. G. dos Remedios and P. D. J. Moens, *J. Struct. Biol.*, 1995, **115**, 175-185.
- 19 M. Y. Berezin and S. Achilefu, *Chem. Rev.*, 2010, **110**, 2641-2684.
- 20 A. Hawe, M. Sutter and W. Jiskoot, *Pharm. Res.*, 2008, **25**, 1487-1499.
- 21 E. Pines, D. Huppert and N. Agmon, *J. Chem. Phys.*, 1988, **88**, 5620-5630.
- 22 N. Amdursky, R. Simkovitch and D. Huppert, *J. Phys. Chem. B*, 2014, **118**, 13859-13869.
- 23 R. Simkovitch and D. Huppert, *J. Phys. Chem. A*, 2015, **119**, 641-651.
- 24 R. Simkovitch and D. Huppert, *J. Phys. Chem. A*, 2015, **119**, 1973-1982.
- 25 M. Dockal, D. C. Carter and F. Ruker, *J. Biol. Chem.*, 2000, **275**, 3042-3050.
- 26 N. El Kadi, N. Taulier, J. Y. Le Huerou, M. Gindre, W. Urbach, I. Nwigwe, P. C. Kahn and M. Waks, *Biophys. J.*, 2006, **91**, 3397-3404.

- 27 M. Suzukida, H. P. Le, F. Shahid, R. A. McPherson, E. R. Birnbaum and D. W. Darnall, *Biochemistry*, 1983, **22**, 2415-2420.
- 28 P. J. Sadler and A. Tucker, *Eur. J. Biochem.*, 1993, **212**, 811-817.
- 29 N. Agmon, *J. Phys. Chem. A*, 2005, **109**, 13-35.
- 30 M. Bhattacharya, N. Jain and S. Mukhopadhyay, *J. Phys. Chem. B*, 2011, **115**, 4195-4205.
- 31 M. Bhattacharya, N. Jain, K. Bhasne, V. Kumari and S. Mukhopadhyay, *J. Fluoresc.*, 2011, **21**, 1083-1090.
- 32 L. R. S. Barbosa, M. G. Ortore, F. Spinozzi, P. Mariani, S. Bernstorff and R. Itri, *Biophys. J.*, 2010, **98**, 147-157.
- 33 B. Cohen, C. Martin Alvarez, N. Alarcos Carmona, J. Angel Organero and A. Douhal, *J. Phys. Chem. B*, 2011, **115**, 7637-7647.
- 34 M. Gutman, D. Huppert and E. Nachliel, *Eur. J. Biochem.*, 1982, **121**, 637-642.
- 35 J. Steinhardt, J. Krijn and J. G. Leidy, *Biochemistry*, 1971, **10**, 4005-4015.
- 36 L. Stryer, *J. Mol. Biol.*, 1965, **13**, 482-495.
- 37 G. V. Semisotnov, N. A. Rodionova, O. I. Razgulyaev, V. N. Uversky, A. F. Gripas and R. I. Gilmanshin, *Biopolymers*, 1991, **31**, 119-128.
- 38 E. Schönbrunn, S. Eschenburg, K. Luger, W. Kabsch and N. Amrhein, *Proc. Natl. Acad. Sci.*, 2000, **97**, 6345-6349.
- 39 D. Togashi and A. Ryder, *J. Fluoresc.*, 2006, **16**, 153-160.
- 40 A. Qadeer, G. Rabbani, N. Zaidi, E. Ahmad, J. M. Khan and R. H. Khan, *Plos One*, 2012, **7**.
- 41 D. Matulis, C. G. Baumann, V. A. Bloomfield and R. E. Lovrien, *Biopolymers*, 1999, **49**, 451-458.
- 42 N. K. Holm, S. K. Jespersen, L. V. Thomassen, T. Y. Wolff, P. Sehgal, L. A. Thomsen, G. Christiansen, C. B. Andersen, A. D. Knudsen and D. E. Otzen, *Biochim. Biophys. Acta, Proteins Proteomics*, 2007, **1774**, 1128-1138.
- 43 J. Juarez, S. Goy Lopez, A. Cambon, P. Taboada and V. Mosquera, *J. Phys. Chem. B*, 2009, **113**, 10521-10529.
- 44 J. Juarez, P. Taboada and V. Mosquera, *Biophys. J.*, 2009, **96**, 2353-2370.
- 45 M. Biancalana and S. Koide, *Biochim. Biophys. Acta, Proteins Proteomics*, 2010, **1804**, 1405-1412.
- 46 N. Amdursky, Y. Erez and D. Huppert, *Acc. Chem. Res.*, 2012, **45**, 1548-1557.
- 47 C. Louis-Jeune, M. A. Andrade-Navarro and C. Perez-Iratxeta, *Proteins Struct. Funct. Bioinf.*, 2012, **80**, 374-381.
- 48 M. W. Amjad, M. C. I. M. Amin, S. M. Mahali, H. Katas, I. Ismail, M. N. ul Hassan and V. T. G. Chuang, *Plos One*, 2014, **9**.
- 49 Y. Moriyama, E. Watanabe, K. Kobayashi, H. Harano, E. Inui and K. Takeda, *J. Phys. Chem. B*, 2008, **112**, 16585-16589.
- 50 R. G. Reed, R. C. Feldhoff, O. L. Clute and T. Peters, *Biochemistry*, 1975, **14**, 4578-4583.
- 51 M. Kubista, R. Sjöback, S. Eriksson and B. Albinsson, *Analyst*, 1994, **119**, 417-419.
- 52 H. P. Soroka, R. Simkovitch, A. Kosloff, S. Shomer, A. Pevzner, O. Tzang, R. Tirosh, F. Patolsky and D. Huppert, *J. Phys. Chem. C*, 2013, **117**, 25786-25797.
- 53 V. N. Uversky, D. J. Segel, S. Doniach and A. L. Fink, *Proc. Natl. Acad. Sci.*, 1998, **95**, 5480-5483.
- 54 D. J. Selkoe, *Nature*, 2003, **426**, 900-904.
- 55 T. R. Jahn, M. J. Parker, S. W. Homans and S. E. Radford, *Nat. Struct. Mol. Biol.*, 2006, **13**, 195-201.